

Molecular Simulation of Covalent Bond Dynamics in Liquid Silicon

Richard C. Remsing^{1, a)} and Michael L. Klein^{2, b)}

¹⁾*Department of Chemistry and Chemical Biology, Rutgers University, Piscataway, NJ 08854*

²⁾*Institute for Computational Molecular Science and Department of Chemistry, Temple University, Philadelphia, PA 19122*

Many atomic liquids can form transient covalent bonds reminiscent of those in the corresponding solid states. These directional interactions dictate many important properties of the liquid state, necessitating a quantitative, atomic-scale understanding of bonding in these complex systems. A prototypical example is liquid silicon, wherein transient covalent bonds give rise to local tetrahedral order and consequent non-trivial effects on liquid state thermodynamics and dynamics. To further understand covalent bonding in liquid silicon, and similar liquids, we present an ab initio simulation-based approach for quantifying the structure and dynamics of covalent bonds in condensed phases. Through the examination of structural correlations among silicon nuclei and maximally localized Wannier function centers, we develop a geometric criterion for covalent bonds in liquid Si. We use this to monitor the dynamics of transient covalent bonding in the liquid state and estimate a covalent bond lifetime. We compare covalent bond dynamics to other processes in liquid Si and similar liquids and suggest experiments to measure the covalent bond lifetime.

I. INTRODUCTION

Many metallic and semi-metallic atomic liquids contain significant numbers of dynamic covalent bonds reminiscent of the static bonds formed in the corresponding solid state. The covalent bonds in these liquids are dynamic, readily breaking and forming on molecular timescales, and the characterization of these processes is complicated due to the interplay between electronic and nuclear structures. Such metallic liquids include molten silicon^{1–8}, boron⁹, gallium¹⁰, and hydrogen at high pressure and temperature^{11–16}, as well as many alloys, including those of importance in phase change random access memory materials^{17–19}. These liquids play important roles in fuel cells, catalysis, and electrochemistry, where the dynamic covalent bonds are expected to play an importance role in chemical reactivity²⁰. Many of these liquids are also found in planetary cores^{16,21–25} and understanding their structure and dynamics is of importance to planetary and geophysical sciences.

In all of these fluids, a complete understanding of their properties requires knowledge of the fundamental interactions and timescales governing their chemical and physical transformations. The relative abundance of dynamic covalent bonds is expected to play a role in determining the thermodynamic properties of the liquid state, as well as the kinetics of phase transformations. For example, liquid silicon displays many of the hallmark anomalies found in water, because the covalent bonds in liquid silicon lead to tetrahedral structures, analogous to hydrogen-bonding in water.

Due to the importance of silicon to the semiconductor industry, and technology as a whole, *l*-Si is well-characterized. However, past research has mainly focused

on the structure and thermodynamics of liquid silicon (*l*-Si). In the solid state at ambient conditions, silicon is a covalently-bonded semiconductor in the diamond lattice, and upon melting it undergoes a semiconductor-to-metal transition^{6,26–28}. Early simulations indeed predicted that *l*-Si is metallic, in agreement with experiments, but they also uncovered a non-negligible fraction of covalent bonds that persist in the liquid state^{1–8}. The existence of these remnants of the solid phase were later confirmed through a combination of computer simulations and Compton scattering experiments².

The formation of covalent bonds in the disordered liquid state indicates the presence of a competition between metallic and covalent interactions in silicon. Indeed, a quantitative description of the solid phases of Si necessitates an accurate model for the balance of metallic and covalent interatomic interactions⁶. This competition between metallic and covalent interactions is also predicted to underlie a metallic-to-semimetallic liquid-liquid phase transition in silicon^{5,8,29–31}. In this case, a high density metallic *l*-Si that is dominated by metallic bonding can transition to a low density semimetallic liquid, in which the interatomic interactions are predominantly covalent bonds, albeit transient ones that readily break and reform in response to thermal fluctuations^{5,8,29–31}.

Despite these significant investigations into the structure and thermodynamics of silicon, quantification of the lifetimes of the transient covalent bonds in *l*-Si is lacking. To address this issue, we use ab initio molecular dynamics (AIMD) simulations to characterize covalent bonding kinetics in *l*-Si, which serves as a prototypical liquid-state system with dynamic covalent bonds. After discussing simulation details in the next section, we quantify the structure of transient covalent bonds in *l*-Si and present a geometric covalent bond definition. We then use this definition to quantify the dynamics of covalent bonding in *l*-Si and conclude with a discussion of future directions.

^{a)}rick.remsing@rutgers.edu

^{b)}mike.klein@temple.edu

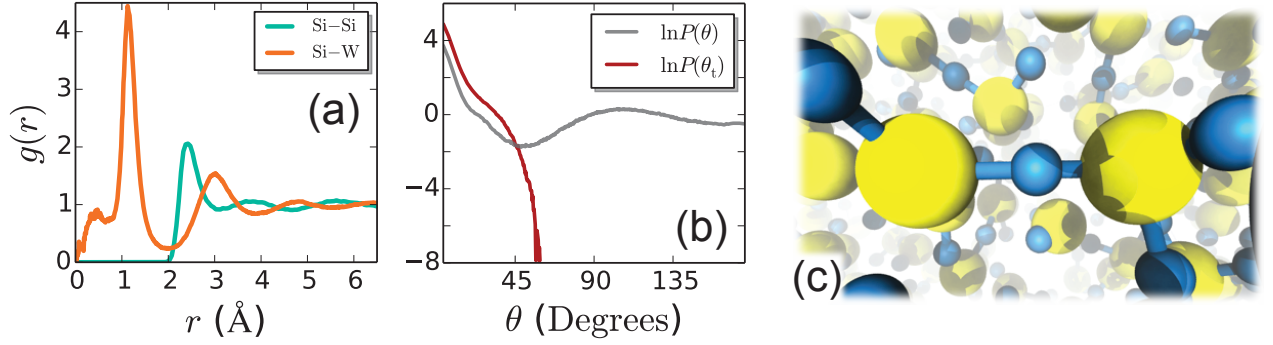


FIG. 1. (a) Pair distribution functions, $g(r)$, for correlations between silicon nuclei (Si-Si) and between silicon atoms and maximally localized Wannier function centers (Si-W). (b) The natural logarithms of the probability distributions of the Si-Si-W angle (θ) and the Si-Si-W angle for triplets involving the additional constraint that the Si-W distance is within the largest peak in the Si-W $g(r)$, $0.75 \text{ \AA} < r_{\text{Si-W}} < 1.75 \text{ \AA}$ (θ_t). The probability distributions are normalized such that they equal unity for a uniform distribution. (c) Snapshot of a Si-Si covalent bond in liquid Si satisfied the geometric definition proposed here. Si atoms are shown in yellow and maximally localized Wannier function centers (W) are shown in blue.

II. SIMULATION DETAILS

We simulated liquid Si at $T = 1800 \text{ K}$ using the CP2K software package following our previous work⁸. The energies and forces in the MD simulations were evaluated using the *QUICKSTEP* module^{32,33}, which employs basis sets of Gaussian-type orbitals and plane waves for the electron density. We used pseudopotentials, to represent the core electrons, and basis sets parameterized by Godecker-Teter-Hutter (GTH): GTH-PADE and GTH double- ζ , single polarization (GTH-DZVP), respectively^{33,34}. We explicitly treated the valence electrons of the 216 Si atoms using the strongly-constrained and appropriately normed (SCAN) meta-generalized gradient approximation (meta-GGA) density functional^{6,35}, as implemented in LIBXC version 4.0.1^{36,37}, with a plane wave cutoff of 650 Ry. Initial configurations were taken from extensively equilibrated simulations performed in earlier work^{7,8}. The systems were then further equilibrated at a constant temperature of $T = 1800 \text{ K}$, maintained using the canonical velocity rescaling thermostat³⁸. Dynamic properties were computed from simulations in the microcanonical ensemble using a timestep of 0.5 fs.

III. COVALENT BOND STRUCTURE IN LIQUID SILICON

We characterize the covalent bond structure in *l*-Si through the calculation of maximally localized Wannier functions (MLWFs) and their centers (MLWFCs)³⁹. MLWFs, in essence, can act as analogs of molecular orbitals for periodic systems, such as crystalline and amorphous solids and liquids, and provide a useful, local picture of chemical bonding^{39,40}. We use the MLWFCs to represent the position of electrons, as done previously^{2,39–43}, in or-

der to quantify electron-nuclei correlations and develop a geometric criterion defining the existence of a covalent bond in an atomic configuration. We note that although the MLWFs themselves are not unique, the MLWFCs are invariant with respect to the choice of gauge within a lattice vector, which is a time-independent constant for simulations in constant volume ensembles, like the microcanonical ensemble used here^{39,44}. Thus, the MLWFCs can be used to define single bonds in each configuration.

We assume that covalent (single) bonds can be accurately defined by considering two- and three-body correlations among Si nuclei and MLWFCs (W). The relevant two-body correlations are encoded in pair distribution functions, $g(r)$, involving Si nuclei and MLWFCs. Three-body correlations are captured by the probability distributions $P(\theta)$, where θ is the Si-Si-MLWFC angle formed by an Si atom, its nearest neighbor Si atom, and a MLWFC. Both sets of distribution functions are shown in Figure 1.

The pair distribution function for Si-Si and Si-MLWFC correlations, shown in Fig. 1a, are consistent with the formation of covalent bonds between Si atoms. The first peak in the Si-W $g(r)$ is located halfway to the first Si-Si peak, and subsequent peaks in the two correlation functions are out of phase. Note that the small peak in the Si-W $g(r)$ at distances less than roughly 1 Å is consistent with the existence of non-bonded, lone pair electrons, visually depicted in Figures 4a-c.

Triplet correlations, as quantified by $P(\theta)$, show that a significant fraction of nearest-neighbor MLWFCs are consistent with covalent bonding, evidenced by the peak in $P(\theta)$ as θ approaches zero (Fig. 1b), consistent with linear Si-MLWFC-Si arrangements. Large values of θ correspond to Si-Si-W triplets not involved in covalent bonds. We additionally consider the possibility that lone pair-like MLWFCs may also appear at low values of θ . Thus, we place the additional constraint on the Si-Si-W

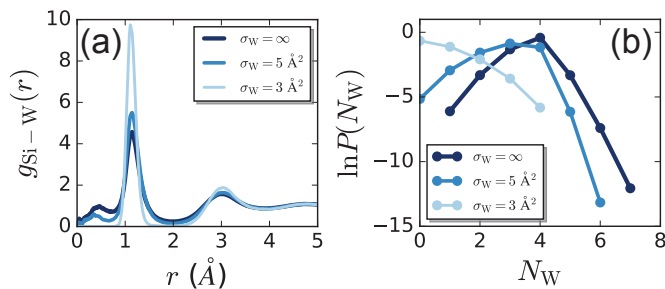


FIG. 2. (a) Pair distribution functions, $g(r)$, for correlations between silicon nuclei and maximally localized Wannier function centers (Si-W) for indicated values of the cutoff for the spread of the MLWFs, σ_W , above which we exclude MLWFs from the calculation. (b) Probability distributions, $P(N_W)$, of the number of MLWFs, N_W , within a distance of 1.75 Å of a central Si atom for the same values of σ_W .

angle that the Si-W distance must be between 0.75 Å and 1.75 Å to avoid counting lone pair MLWFs, resulting in the angle θ_t . This more tightly-constrained angle removes contributions from lone pairs to the angular distribution $P(\theta_t)$, Fig. 1b. With this additional constraint, we suggest a reasonable geometric definition of a Si-Si covalent bond corresponds to a Si-Si distance less than 3 Å and $\theta_t < 30^\circ$. One such covalent bond is highlighted in Fig. 1c.

In the snapshot shown in Fig. 1c, as well as those in Figs. 4a-c, one can observe a range of bonding and coordination environments. In particular, the number of MLWFs associated with a single Si atom varies, and, similarly, the number of Si atoms associated with a MLWFC also varies. Characterizing the fluctuations in Si and MLWFC coordination structures quantifies the probability of forming lone pairs, covalent bond pairs, and metallic or diffuse pairs^{2,9}. However, positional correlations alone do not suffice to characterize the nature of the MLWFs, as discussed above in the context of angular correlations. Lone pairs and covalent bond MLWFs are high localized in space, such that their spreads are small, such that bonded MLWFs are generally more localized than lone pair MLWFs^{2,9}. In contrast, the spreads of metallic or diffuse MLWFs are large, corresponding to delocalized pairs. Therefore, we quantify the coordination structure of Si atoms and MLWFs through distances, as well as a range of MLWF spreads. We introduce a MLWF spread cutoff, σ_W , such that MLWFs with spreads above this value are not included in averages; $\sigma_W = \infty$ indicates that all MLWFs are included in the calculations.

We start by examining the impact of σ_W on the Si-MLWFC pair distribution function, $g_{\text{Si-W}}(r)$, shown in Fig. 2a. Introducing a finite σ_W removes the contribution of diffuse MLWFs from the pair distribution function. A spread cutoff of 5 Å² reduces the peak at small distances and slightly increases the first major peak, as well as the second peak. Further decreasing σ_W to 3 Å² removes

diffuse and nearly all lone pairs, evidence by an absence of a peak for $r < 1 \text{ Å}$. The MLWFs remaining in the calculation are predominantly covalently bonded pairs, and the intensity of the first major peak in $g_{\text{Si-W}}(r)$, corresponding to bonded pairs, increasingly significantly. The second peak increases slightly as well. Therefore, σ_W can be tuned to remove diffuse and lone pair MLWFs, and this tuning has the mainly impacts the structure of the first coordination shell, $r < 1.75 \text{ Å}$.

The probabilities of observing N_W MLWFs in the first coordination shell of an Si atom for various σ_W are shown in Fig. 2b. When all MLWFs are included, N_W ranges from 1-7, and a maximum is observed at $N_W = 4$, as expect from the sp^3 hybridization of the Si atoms. As the cutoff is decreased, $P(N_W)$ shifts toward lower values, as delocalized MLWFs are removed from consideration. For $\sigma_W = 5 \text{ Å}^2$, the maximum shifts to $N_W = 3$, with similar probabilities at $N_W = 2$ and $N_W = 4$. The appearance of finite probability for $N_W = 0$ is consistent with Si atoms that have all their electrons in diffuse, metallic states. Further reduction of σ_W to 3 Å², which limits the set of MLWFs almost entirely to covalently bonded pairs, shifts the maximum of $P(N_W)$ to zero, consistent with a small fraction (roughly 30 percent) of Si atoms involved in covalent bonds. In this limit, $P(N_W)$ essentially corresponds to probability of an Si atom having N_W covalent bonds. This spans zero to four bonds per Si atom, and monotonically decreases with N_W , indicating that Si atoms fully coordinated by covalent bonds are less probable than partially and non-bonded Si atoms. This is consistent with the metallic nature of liquid Si.

We now turn our attention to the coordination structure of the MLWFs, particularly those that are in the first coordination of a Si atom. To quantify this, we compute the joint probability distribution, $P(N_{\text{Si}}, N_W)$, corresponding to the probability that a central Si atom is coordinated by N_W MLWFs and one of those coordinated MLWFs is in turn coordinated by N_{Si} Si atoms (including the central Si atom). A schematic for $N_W = 4$ and $N_{\text{Si}} = 2$ for one MLWFC is shown in Fig. 3a. For ease of visualization, we focus on the conditional probability,

$$P(N_{\text{Si}}|N_W) = \frac{P(N_{\text{Si}}, N_W)}{P(N_W)}, \quad (1)$$

physically corresponding to the probability that a MLWFC in the coordination shell of a central Si atom is coordinated by N_{Si} Si atoms, given that the central Si has N_W MLWFs in its first coordination shell. These distributions are shown in Fig. 3b-c for varying σ_W .

When all MLWFs are included in $P(N_{\text{Si}}|N_W)$, the conditional probability has a maximum at $N_{\text{Si}} = 2$ for all values of $N_W > 1$. This maximum corresponds to a covalent bond between the central Si and a neighboring Si atom. Reducing N_W from 6 to 2 primarily impacts the probably of observing singly coordinated MLWFs (to the central Si), which increases as N_W is lowered. For $N_W = 1$, $P(N_{\text{Si}}|N_W)$ differs significantly from the

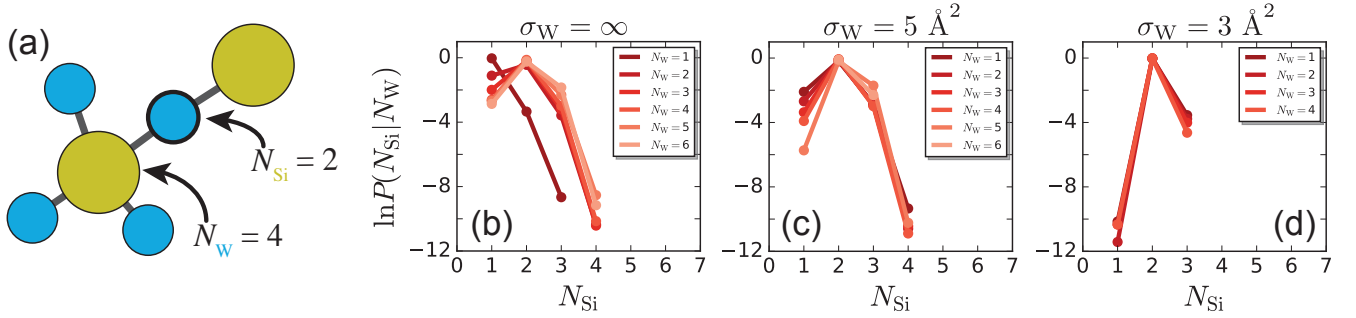


FIG. 3. (a) Schematic diagram indicating the examples of N_W and the number of Si atoms around a MLWFC that is in the coordination shell of a Si atom, N_{Si} . Si atoms are colored yellow and MLWFCs are colored blue. Arrows point toward the Si and MLWFC to which the indicated N_W and N_{Si} refer. (b-d) Conditional probability distributions, $P(N_{Si}|N_W)$, of the number of Si atoms within a distance of 1.75 \AA of a MLWFC, where the MLWFC is part of a Si coordination shell composed of N_W MLWFCs, for the indicated values of the MLWFC spread cutoff, σ_W .

rest, with $N_{Si} = 1$ being most probable, indicating that the MLWFC is most likely a diffuse or lone pair.

Introducing a finite MLWF spread cutoff of $\sigma_W = 5 \text{ \AA}^2$ removes diffuse pairs and results in distributions that are similar for all N_{Si} , except $N_{Si} = 1$. As N_W is decreased, the probability of observing singly-coordinated, lone pair MLWFCs increases. Further reduction of σ_W to 3 \AA^2 results in sharp $P(N_{Si}|N_W)$ distributions that are nearly independent of N_W . These distributions span $1 \leq N_{Si} \leq 3$, with a large maximum at $N_{Si} = 2$, corresponding to covalent bond MLWFCs. We note that there is a small probability for lone pairs when $\sigma_W = 3 \text{ \AA}^2$, but lowering the spread cutoff further will increasingly remove these MLWFCs and select only covalently bonded pairs^{2,9}.

In summary, the local (bonding) coordination structure of Si atoms significantly fluctuates and involves diffuse metallic, lone pair, and covalently-bonded states. We have characterized these states, and the use of a MLWF spread cutoff, σ_W , can be used to systematically tune the involvement of these states when necessary. Alternatively, Si-Si-W angular correlations, in addition to Si-Si and Si-W distances, used in the above-described geometric definition of covalent bonds can be used to uncover covalently-bonded MLWFCs in a similar manner, because linear Si-W-Si structures are consistent with $N_{Si} = 2$ covalently-bonded pairs.

IV. COVALENT BOND DYNAMICS IN LIQUID SILICON

Our simulations suggest that covalent bonds in *l*-Si rapidly break and reform on sub-picosecond timescales. Figures 4a-c highlight one such covalent bond breakage and reformation event. There, we show the time evolution of the MLWFCs (blue spheres) for the atoms involved in the highlighted covalent bond exchange. Initially (a), the central yellow Si atom is bonded to the left pink Si atom; a linear Si-MLWFC-Si structure indicates a single covalent bond expected from the sp^3 hybridiza-

tion of Si. This bond breaks at a later time (b) due to thermal fluctuations, before the MLWFC of the central Si rotates and forms a new bond with the rightmost red Si (c).

Using the geometric definition of a covalent bond described in the previous section, we are able to quantify the kinetics of Si-Si bond breakage, in a manner analogous to conventional approaches to characterizing hydrogen bond dynamics in water^{45–47}, and, more recently, halogen bond dynamics in solid and liquid chlorine^{41,43}. To do so, we define an indicator function, $h(t)$, which is equal to one when a covalent bond is present and zero otherwise. We quantify covalent bond kinetics through the reactive flux correlation function⁴⁵

$$k(t) = -\frac{dC(t)}{dt} = -\frac{\langle \dot{h}(0) [1 - h(t)] \rangle}{\langle h \rangle}, \quad (2)$$

where $C(t)$ is the time correlation function (TCF) characterizing covalent bond lifetimes,

$$C(t) = \frac{\langle h(t)h(0) \rangle}{\langle h \rangle}. \quad (3)$$

The reactive flux correlation function, $k(t)$, is shown in Figure 4d. At short times, vibrational and librational motion manifest the non-trivial, transient behavior on scales less than roughly 0.3 ps . Beyond this time period, $k(t)$ decays in a manner consistent with first-order kinetics, $k(t) \sim \tau^{-1} \exp(t/\tau)$, where $\tau \approx 0.6 \text{ ps}$ is the covalent bond lifetime estimated from fitting to the long-time behavior of $k(t)$, shown as a dashed line in Fig. 4d.

The covalent bond lifetime estimated above is similar to other significant timescales in *l*-Si. Orientational correlations, the velocity autocorrelation function, and self-intermediate scattering functions all decay on timescales similar to the covalent bond lifetime^{7,8}. The agreement among various structural relaxation times and the covalent bond lifetime suggests that covalent bond breakage is a limiting step for structural relaxation. This may be

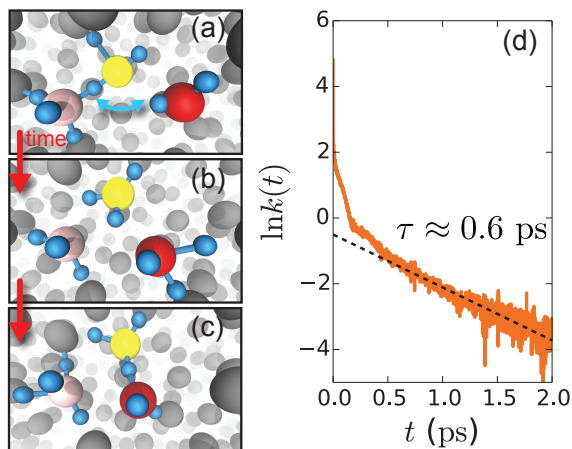


FIG. 4. (a-c) Snapshots of covalent bond breakage and reformation in liquid silicon, with three Si atoms involved in the events colored yellow, pink, and red; all other Si atoms are colored grey. Maximally localized Wannier function centers (MLWFCs) associated with the colored silicon atoms are shown in blue. (a) Initially, the central (yellow) Si is bonded to the pink Si atom on the left, as indicated by the lines connecting the Si atoms through a bridging MLWFC. (b) At some time later, the bond breaks due to thermal fluctuations, and the MLWFC does not connect to Si atoms. (c) A new bond then forms between the central Si atom and the rightmost (red) colored Si atom. The left (pink) Si has also formed a new bond on this timescale. (d) The kinetics of bond covalent bond breakage is quantified by the reactive flux correlation function, $k(t)$, and fitting its long time behavior (dashed line) results in a covalent bond lifetime of $\tau \approx 0.6$ ps.

expected from the strength of covalent bonds, as well as their propensity to create local tetrahedral order in the liquid state.

V. CONCLUSIONS

In this work, we have presented an approach to estimate the lifetimes of transient covalent bonds in condensed phase systems with an application to liquid silicon. The general strategy utilizes a maximally localized Wannier function (MLWF) approach to chemical bonding, such that the existence of a covalent bond can be defined using two-body Si-Si correlations and three-body correlations involving two Si nuclei and the center of a MLWF. With this geometric, *ab initio* definition of a covalent bond, we can estimate covalent bond lifetimes in the liquid state from equilibrium simulations using the reactive flux formalism. For liquid silicon at 1800 K and ambient pressure, we estimate a covalent bond lifetime of $\tau \approx 0.6$ ps. We note, however, that the generic concept of monitoring bond dynamics using a geometric, electronic structure-based bond definition is not limited to equilibrium and could be used to monitor covalent bond dynamics in melting or freezing processes at the focus of

laster melting experiments^{30,48,49}, for example.

The covalent bond lifetime in liquid silicon may be measured using time-dependent scattering measurements, such as a time-dependent Compton scattering. Compton scattering has been used to shed light on the average bonding properties of metallic liquids^{2,9}. Extensions of this technique to the time domain are expected to uncover similar information about the average dynamic properties of transient covalent bonds, like the lifetime at the focus of this work^{50–52}.

Finally, we note that the covalent bond lifetime in *l*-Si is similar to bond lifetimes in other conventional liquids with directional attractive interactions. The hydrogen bond lifetime in liquid water is on the picosecond timescale^{46,47}, as is the halogen bond lifetime in liquid Cl₂⁴¹. Despite the vast differences in these liquids, their directional bonds all share a common thread: the strength of the isolated bond, which is significantly weakened in the condensed phase, is on the order of $10k_B T$ at the temperature of the respective liquids⁵³. Thus, thermal fluctuations in each of these different liquids are large enough to cause the directional attractions to exist only fleetingly, highlighting qualitative similarities of directional bond dynamics in the liquid state.

ACKNOWLEDGMENTS

This work was supported as part of the Center for Complex Materials from First Principles (CCM), an Energy Frontier Research Center funded by the U.S. Department of Energy, Office of Science, Basic Energy Sciences under Award #DE-SC0012575. Computational resources were supported in part by the National Science Foundation through major research instrumentation grant number 1625061 and by the US ARL under contract number W911NF-16-2-0189.

- ¹I. Štich, R. Car, and M. Parrinello, Phys. Rev. B **44**, 4262 (1991).
- ²J. T. Okada, P. H.-L. Sit, Y. Watanabe, Y. J. Wang, B. Barbiellini, T. Ishikawa, M. Itou, Y. Sakurai, A. Bansil, R. Ishikawa, M. Hamaishi, T. Masaki, P.-F. Paradis, K. Kimura, T. Ishikawa, and S. Nanao, Phys. Rev. Lett. **108**, 067402 (2012).
- ³I. Štich, M. Parrinello, and J. M. Holender, Phys. Rev. Lett. **76**, 2077 (1996).
- ⁴I. Štich, R. Car, and M. Parrinello, Phys. Rev. Lett. **63**, 2240 (1989).
- ⁵S. S. Ashwin, U. V. Waghmare, and S. Sastry, Phys Rev Lett **92**, 175701 (2004).
- ⁶J. Sun, R. C. Remsing, Y. Zhang, Z. Sun, A. Ruzsinszky, H. Peng, Z. Yang, A. Paul, U. Waghmare, X. Wu, M. L. Klein, and J. P. Perdew, Nat Chem **8**, 831 (2016).
- ⁷R. C. Remsing, M. L. Klein, and J. Sun, Phys. Rev. B **96**, 024203 (2017).
- ⁸R. C. Remsing, M. L. Klein, and J. Sun, Phys. Rev. B **97**, 140103(R) (2018).
- ⁹J. Okada, P.-L. Sit, Y. Watanabe, B. Barbiellini, T. Ishikawa, Y. Wang, M. Itou, Y. Sakurai, A. Bansil, R. Ishikawa, and et al., Phys. Rev. Lett. **114**, 177401 (2015).
- ¹⁰X. G. Gong, G. L. Chiarotti, M. Parrinello, and E. Tosatti, Europhys. Lett. **21**, 469 (1993).
- ¹¹G. Rillo, M. A. Morales, D. M. Ceperley, and C. Pierleoni, Proceedings of the National Academy of Sciences **116**, 9770 (2019).

- ¹²M. A. Morales, J. M. McMahon, C. Pierleoni, and D. M. Ceperley, *Physical Review Letters* **110** (2013), 10.1103/physrevlett.110.065702.
- ¹³C. Pierleoni, M. Holzmann, and D. M. Ceperley, *Contributions to Plasma Physics* **58**, 99 (2017).
- ¹⁴C. Pierleoni, M. A. Morales, G. Rillo, M. Holzmann, and D. M. Ceperley, *Proceedings of the National Academy of Sciences* **113**, 4953 (2016).
- ¹⁵C. Pierleoni, G. Rillo, D. M. Ceperley, and M. Holzmann, *Journal of Physics: Conference Series* **1136**, 012005 (2018).
- ¹⁶M. Zaghoo and I. F. Silvera, *Proceedings of the National Academy of Sciences* **114**, 11873 (2017).
- ¹⁷T. H. Lee and S. R. Elliott, *Adv. Mater.* **29**, 1700814 (2017).
- ¹⁸D. Loke, T. H. Lee, W. J. Wang, L. P. Shi, R. Zhao, Y. C. Yeo, T. C. Chong, and S. R. Elliott, *Science* **336**, 1566 (2012).
- ¹⁹J. M. Skelton, D. Loke, T. Lee, and S. R. Elliott, *ACS Appl. Mater. Interfaces* **7**, 14223 (2015).
- ²⁰A. Zavabeti, J. Z. Ou, B. J. Carey, N. Syed, R. Orrell-Trigg, E. L. H. Mayes, C. Xu, O. Kavehei, A. P. O'Mullane, R. B. Kaner, K. Kalantar-zadeh, and T. Daeneke, *Science* **358**, 332 (2017).
- ²¹J. Paul Poirier, *Phys. Earth Planet. Inter.* **85**, 319 (1994).
- ²²M. Pozzo, C. Davies, D. Gubbins, and D. Alfè, *Physical Review B* **87** (2013), 10.1103/physrevb.87.014110.
- ²³M. Pozzo, C. Davies, D. Gubbins, and D. Alfè, *Earth Planet. Sci. Lett.* **393**, 159 (2014).
- ²⁴Q. Williams, *Annu. Rev. Earth Planet. Sci.* **46**, 47 (2018).
- ²⁵G. Mazzola, R. Helled, and S. Sorella, *Physical Review Letters* **120** (2018), 10.1103/physrevlett.120.025701.
- ²⁶O. Sugino and R. Car, *Phys. Rev. Lett.* **74**, 1823 (1995).
- ²⁷D. Alfè and M. J. Gillan, *Phys. Rev. B* **68**, 205212 (2003).
- ²⁸P. F. McMillan, M. Wilson, D. Daisenberger, and D. Machon, *Nat Mater* **4**, 680 (2005).
- ²⁹P. Ganesh and M. Widom, *Phys Rev Lett* **102**, 075701 (2009).
- ³⁰M. Beye, F. Sorgenfrei, W. F. Schlotter, W. Wurth, and A. Föhlisch, *Proc Natl Acad Sci U S A* **107**, 16772 (2010).
- ³¹S. Sastry, *Proc Natl Acad Sci U S A* **107**, 17063 (2010).
- ³²J. VandeVondele, M. Krack, F. Mohamed, M. Parrinello, T. Chassaing, and J. Hutter, *Comput. Phys. Commun.* **167**, 103 (2005).
- ³³J. VandeVondele and J. Hutter, *J. Chem. Phys.* **127**, 114105 (2007).
- ³⁴S. Goedecker, M. Teter, and J. Hutter, *Phys. Rev. B* **54**, 1703 (1996).
- ³⁵J. Sun, A. Ruzsinszky, and J. P. Perdew, *Phys. Rev. Lett.* **115**, 036402 (2015).
- ³⁶S. Lehtola, C. Steigemann, M. J. Oliveira, and M. A. Marques, *SoftwareX* **7**, 1 (2018).
- ³⁷M. A. Marques, M. J. Oliveira, and T. Burnus, *Computer Physics Communications* **183**, 2272 (2012).
- ³⁸G. Bussi, D. Donadio, and M. Parrinello, *J. Chem. Phys.* **126**, 014101 (2007).
- ³⁹N. Marzari, A. A. Mostofi, J. R. Yates, I. Souza, and D. Vanderbilt, *Rev. Mod. Phys.* **84**, 1419 (2012).
- ⁴⁰P. L. Silvestrelli, N. Marzari, D. Vanderbilt, and M. Parrinello, *Solid State Commun.* **107**, 7 (1998).
- ⁴¹R. C. Remsing and M. L. Klein, *J. Phys. Chem. B* **123**, 6266 (2019).
- ⁴²R. C. Remsing, J. Sun, U. V. Waghmare, and M. L. Klein, *Mol. Phys.* **116**, 3372 (2018).
- ⁴³R. C. Remsing and M. L. Klein, *Phys. Rev. Lett.* **124**, 066001 (2020).
- ⁴⁴E. Blount, in *Solid state physics*, Vol. 13 (Elsevier, 1962) pp. 305–373.
- ⁴⁵D. Chandler, *J. Chem. Phys.* **68**, 2959 (1978).
- ⁴⁶A. Luzar, *J. Chem. Phys.* **113**, 10663 (2000).
- ⁴⁷A. Luzar and D. Chandler, *Nature* **379**, 55 (1996).
- ⁴⁸S. R. Stiffler, M. O. Thompson, and P. S. Peercy, *Phys Rev Lett* **60**, 2519 (1988).
- ⁴⁹P. G. Sanders and M. J. Aziz, *J. Appl. Phys.* **86**, 4258 (1999).
- ⁵⁰R. E. Wagner, Q. Su, and R. Grobe, *Phys. Rev. A* **82**, 022719 (2010).
- ⁵¹A. F. Kemper, M. Sentef, B. Moritz, C. C. Kao, Z. X. Shen, J. K. Freericks, and T. P. Devereaux, *Phys. Rev. B* **87**, 235139 (2013).
- ⁵²M. Grosser, J. M. Slowik, and R. Santra, *Phys. Rev. A* **95**, 062107 (2017).
- ⁵³R. G. Bryant, M. A. Johnson, and P. J. Rossky, *Acc. Chem. Res.* **45**, 1 (2012).